Desorption Mechanism of a Pesticide from a Hydrated Calcium Montmorillonite Unraveled by Molecular Dynamics Simulations

Bastien Belzunces, Sophie Hoyau, Jérôme Cuny, Fabienne Bessac

Desorption Mechanism of a Pesticide from an Hydrated Calcium Montmorillonite Unraveled by Molecular Dynamics Simulations.

Bastien Belzunces,[†] Sophie Hoyau,[†] Jérôme Cuny,[†] and Fabienne Bessac[*,‡,†]

†*Laboratoire de Chimie et Physique Quantiques, 118 route de Narbonne, Université de Toulouse, UPS, CNRS (UMR 5626), Toulouse, F-31062, France*

‡*Ecole d'ingénieurs de Purpan, Université de Toulouse, Toulouse INP, 75 voie du TOEC, BP 57611, Toulouse Cedex 03, F-31076, France*

E-mail: fabienne.bessac@purpan.fr

Phone: +33 (0)7 62062786. Fax: +33 (0)5 61153060

Abstract

Fenhexamid, N-(2,3-dichloro-4-hydroxyphenyl)-1-methylcyclohexanecarboxamide, a fungicide, is authorized in the European Union to be used in agriculture. Active molecule behavior in the environment and their transfer to environmental components (soil, water and air) are primordial topics to study to limit environmental pollution. Following a step by step approach, we studied fenhexamid. In previous works, we worked on the fenhexamid pesticide isolated, then on its complexes with one or two Ca^{2+} and Na^{+}, the most abundant cations into soils, in the gas phase. We also reported theoretical calculations about fenhexamid in interaction with a clay surface: a Ca–montmorillonite. In the present paper, potentials of mean force describing overall fenhexamid desorption from a Ca–montmorillonite surface in presence of water were

computed from molecular dynamics simulations combined with umbrella sampling. Several mechanisms were envisaged. The results allow to quantitatively estimate the free energy of desorption and to provide a detailed insight into the hydration sphere of Ca^{2+} during the desorption process.

Introduction

The development of water resources is a major issue regarding the impacts of climate change, population flows (tourism, urban sprawl), epidemics, etc. All uses of water are concerned: drinking water supply and sanitation, agricultural and industrial uses. However, these water resources are often contaminated with many organic compounds. In this context, studying the behavior of organic contaminants such as pesticides (PEST) in water and the interactions between these contaminants and natural inorganic substrates such as clay is of paramount importance. The process of pesticide desorption from clay is not easy to monitor experimentally, while computational chemistry can provide significant input into soil and water contaminant behavior. Several pesticides (atrazine, metamitron, fenhexamid...) have already been studied in our group. The global project is carried out using a step by step approach. The pesticide is considered: (i) isolated and (ii) in interaction with cations[1–3]; (iii) in interaction with soil surfaces[4,5]; (iv) all the previous systems are currently studied in the presence of water. The present work concerns more particularly the fenhexamid pesticide. Smectite clay minerals are abundant in soils and have very interesting properties as high swelling behavior, high surface area, large negative charge... Due to those properties, smectites are used as catalysts, sorbents and barriers for contaminants (radioactive waste repositories)... Montmorillonite family belongs to smectite type and shares basic structure with pyrophyllite, an aluminum phyllosilicate of formula: $Al_2(Si_4O_{10})(OH)_2$ organized in layers. Temperature ramp experiments measuring the weight loss of water from smectite type of clay have shown at least two kinds of interlayer water in smectites[6–9]. A first type of water is readily removable through drying or heating, a second kind of water is more

strongly bound. Water lost below 150°C is assigned to bulk and weakly bound water. The highest peak temperatures for magnesium, calcium, strontium, barium, and lithium clay are found to correlate with the hydration energies of the cations and are related to the interaction of the clay with the cation. About six water molecules per cation was found, at the first step of hydration for divalent cations, and about three water molecules for lithium and sodium cations. In addition, in montmorillonite (Mont), IR experiments have shown that spectral absorptions due to water molecules are influenced by both the interlayer cation and the moisture content[9–11]. First, adsorbed water on Mont solvates the cationic counterions. Trends in the sorbed amount of water, swelling properties, and the enthalpy of hydration have led to deduce that the principal mechanism underlying the observed variations is the hydration of the cationic counterions.

In different theoretical works on pyrophyllite[12] and montmorillonite[13–16], the water contents were varied in order to get insight into swelling mechanisms and into the cation hydration state when the moisture content increases. In particular, Holmboe group studied cation hydration in the interlayer of Na–Mont and Ca–Mont going from dry clay (0W), up to the tenth-layer hydrate called 10W using CLAYFF force field Molecular Dynamics (MD) simulations (see Table 1)[17,18]. For Ca–Mont, at 1W in the basal spacing d_{001} of about 13.7 Å, Ca^{2+} are close to the Mont surface and hydrated by 7 water molecules which are not spherically distributed around Ca^{2+}. From 2W to higher hydration states, Ca^{2+} are surrounded by 8 water molecules in their first hydration sphere (HS) but only from the 3W hydrate state, Ca^{2+} are hydrated with an evenly distributed spherical first coordination sphere. At the 5W hydration state, the basal spacing d_{001} is equal to $\approx$ 24.8 Å for both Na–Mont and Ca–Mont.

Table 1: Water contents and basal spacing, d_{001}, for different hydrate states of Mont. NW: Nth-layer hydrate state and n: number of water molecules per unit cell per layer-hydrate[17,18].

NW	0W	1W	2W	3W	4W	5W	10W
d_{001} (Å)	9.5-10.1	12.0-12.7	15.0-15.7	18.0-19.0	21.4-22.0	≈24.8	≈40.7
n	0	5	10	15	20	25	50

The geometrical structure and energetics of hydrated Ca^{2+} have also been studied in vacuum by theoretical calculations or *via* EXAFS neutron diffraction experiments[19]. Coordination numbers of 6, 7 and 8 are common for the first HS of Ca^{2+}. For hydrated structures of the form $Ca(H_2O)_i^{2+}.jH_2O$, i water molecules are in the first coordination sphere and j water molecules are in the second coordination sphere (hydrogen bonded to water molecules in the first sphere). The clusters $Ca(H_2O)_4^{2+}.2H_2O$ and $Ca(H_2O)_5^{2+}.1H_2O$ were significantly higher in relative energy than $Ca(H_2O)_6^{2+}$ (> 8 kcal.mol^{-1})[20,21]. On the contrary, $Ca(H_2O)_6^{2+}.2H_2O$, $Ca(H_2O)_7^{2+}.1H_2O$ or $Ca(H_2O)_8^{2+}$ were in the same range of energy (relative energies < 2 kcal.mol^{-1})[20,21]. Moreover, the first HS was found to be long-lived at room temperature (300 K). Half of the initial solvating water molecules are still in the HS after 1 ns of simulation time (Car-Parrinello MD within the NVT ensemble using the hybrid DFT functional B3LYP). In contrast, at higher temperature, 500 K, frequent exchanges are observed between HS. At 900 K, the rate of exchanges is raised to a great extent compared to 300 K. In average, the residence time is estimated to be between 0 and 6.4 ps[22].

Water adsorption on Mont surface is greatly influenced by the cationic counterions just like organic molecule adsorption on Mont is greatly influenced by the cationic counterions and the water loading of Mont interlayer space. Due to Mont adsorption properties, this clay family has been considered as highly efficient materials for the removal of contaminants such as pesticides from wastewater. Mont combines several strengths: it is inexpensive, environmentally friendly, abundant and efficient to adsorb a wide range of contaminant types[23]. Theoretical groups have previously been working on adsorption of small organic molecules on Mont. Among them, Mignon *et al.* have studied DNA bases adsorption energies on dry Na–Mont[24,25], and cytosine adsorption on hydrated Na–Mont[26] with *ab initio* MD simulations; Szczerba *et al.* have performed force field molecular dynamics simulations in order to study the interactions of ethylene glycol with watered smectite (Ca–Mont)[27]; Aggarwal *et al.* have used force field quantum mechanics to estimate relative energies for the adsorption of non-ionic organic solutes in clay mineral-water-solute systems (K–Mont)[28]; Clausen *et al.* have

investigated the adsorption of single molecules of volatiles, such as water, ethanol, ethyl acetate, pyridine, toluene, and n-octane, on the dry surface of a smectite clay (Na–Mont) using DFT MD[29]; sorption of the anionic form of the 2,4–D pesticide (2,4–dichlorophenoxyacetic acid) on dry and hydrated surfaces of a Ca–montmorillonite has been investigated using *ab initio* molecular dynamics simulation at room temperature[30]; carbon dioxide intercalation in hydrated Na–montmorillonite has also been under investigations[31].

To the authors' knowledge, one other work in scientific literature reports the combination of MD and umbrella sampling to compute the desorption of organic molecules, paracetamol and carbamazepine, from a watered clay surface, Na–saponite. This study was made in the force field framework using LAMMPS software.[32] Moreover, prior DFT researches using umbrella sampling to understand adsorption and desorption mechanisms on surfaces and bulk systems have been conducted, for instance: (i) the exploration of the free-energy profile of dimethylamine at the air–water surface[33]; (ii) the degradation of diisopropyl methylphosphonate on $\gamma - Al_2O_3$ surface[34]. The present work is more ambitious and allows the quantitative estimation of the free energy of desorption of the fenhexamid (Fen, see Figure 1) from a Ca–Mont clay surface in presence of water within the DFT framework. Fen is a fungicide for preventive use against Botrytis cinerea, the agent of gray rot. After a brief presentation of

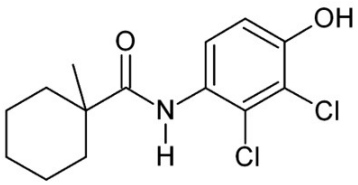

Figure 1: Structural formula of the fenhexamid, $C_{14}H_{17}Cl_2NO_2$.

the theoretical tools, we present the different mechanisms for the desorption of a pesticide from the Ca–Mont surface. The free energy profiles of desorption were calculated. The different alternatives are compared energetically and highlighting the importance of Ca^{2+} hydration.

Methods

Montmorillonite model

Phyllosilicates designate minerals in which tetrahedral (T) and octahedral (O) sheets are stacked successively. Tetrahedron and octahedron vertices are oxygen (O^{2-}) and hydroxyl (OH^{-}). Montmorillonite, a 2:1 phyllosilicate (T/O/T), is a dioctahedral smectite (see Figure 2):

- in T sheets, Si^{4+} cations occupy all sites;
- in O sheets, two thirds of the octahedral sites are occupied by Al^{3+}.

Isomorphic substitutions can occur in both T and O sheets but are naturally more abundant in the O sheet. Consequently, montmorillonite interlayer space contains cationic counterions to compensate the net negative charge of the clay. The montmorillonite model we worked with had the following characteristics:

- $\approx$16.7% of substitutions of Al^{3+} by Mg^{2+} in O sheets;
- no substitution in T sheets;
- Ca^{2+} compensating cations in the interlayer.

X-ray data from Wardle *et al.*[35] on pyrophyllite (2:1 dioctahedral smectite with neither substitution, nor interlayer compensating cation) was our starting point to build Mont model. Unit cell parameters (a, b, c, α, β and γ) optimized at PBE-D2 level were in very good agreement with experimental data (see previous works[4,5]). The triclinic computational cell consisted of six pyrophyllite unit cell (3a$\times$2b$\times$c) in order to accommodate fenhexamid pesticide in the interlayer. Four Al^{3+} were substituted by Mg^{2+} in O sheets, and the resultant negative charge was compensated by two Ca^{2+} cations in the interlayer. In a previous work, we showed that Fen interacts with only one cation[5]. In the following, the Ca^{2+} in interaction with the pesticide is noted Ca1 while Ca2 designates the Ca^{2+}, which does not interact

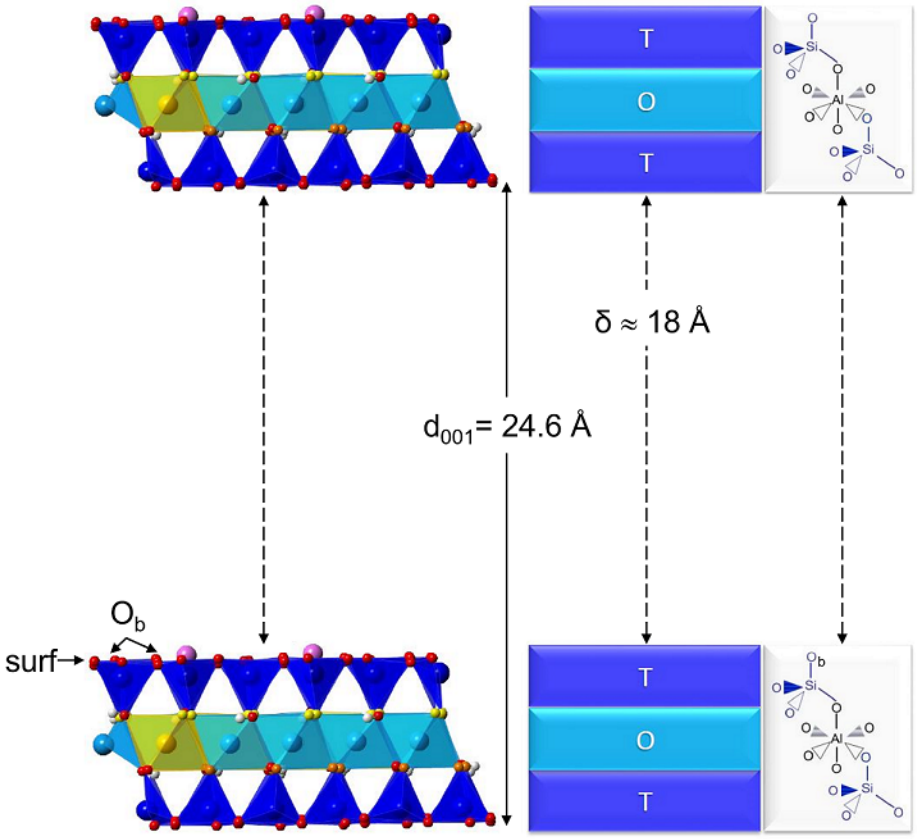

Figure 2: Montmorillonite representation. Mont contains 4 substitutions of Al^{3+} (ligth blue) by Mg^{2+} (yellow) in the O sheet and 2 Ca^{2+} cations (magenta) compensate the net negative charge carried by the clay layer and are situated above substitutions (ditrigonal ring of basal oxygens, Ob). The whole set of Ob atoms forms Mont surface, noted surf. Si ions in the T sheet are in dark blue. δ designates the interlayer spacing and d_{001}, the basal spacing.

with the pesticide. In the following, computational cell parameters were set to: 15.500 Å× 17.931 Å× 25.000 Å and α= 91.030°, β= 100.374°, γ= 89.757°; and were kept fixed during molecular dynamics simulations. The basal spacing d_{001} =csinβ is equal to 24.6 Å.

CPMD parameters

Car-Parrinello molecular dynamics simulations[36] were performed under periodic boundary conditions using the Perdew-Burke-Ernzerhof (PBE)[37–41] functional as implemented in the CPMD package[42]. The D2 Grimme's dispersion correction[43–45] has been added (PBE-D2). Valence-core interactions have been described using Troullier-Martins norm-conserving pseu-

dopotentials[46,47] in combination with a plane-wave basis set. The cut-off energy for plane waves is 80 Ry and the Monkhorst-Pack method[48] was used to sample the Brillouin zone at the Γ point only within the triclinic computational cell. Hydrogen atoms were replaced by deuterium atoms. The fictitious mass of the electrons was $\mu = 500$ $a.u.$ and the time step 4.5 $a.u.$. Hydrated Fen–Ca–Mont starting point originates from a 12 ps molecular dynamics (MD) trajectory performed within the NVT ensemble with a Langevin thermostat[49] at 350 K[50–52]. 132 water molecules are present in the interlayer space measuring around ≈18 Å in all the trajectories of this work. These conditions corresponds to the 5W hydrate state qualified by Holmboe and coworkers at 298 K (see Table 1)[17,18]. To model the desorption of Fen from the hydrated surface of Mont, the Umbrella Sampling method[53–55] was implemented. Eleven biased Car-Parrinello molecular dynamics simulations were conducted to move the system under study from one thermodynamically stable state to another following a reaction coordinate noted ξ (see Table 2). PLUMED, an open-source, community-developed library was used to bias the trajectories[56–58]. The simulations lasted between 11 and 25 ps. An equilibration time of 4 ps was removed from the analysis for each simulation. With the eleven trajectories, a total duration of 177 ps was simulated.

Fen desorption from watered Ca–Mont has been quantified by deriving the potential of mean force (PMF). The PMF characterizes the change in the free energy of the system due to the changes in its configuration[59–62]. The free energy F of a system in thermodynamic equilibrium in an NVT statistical ensemble is defined as:

$$F = -k_B T ln Z \tag{1}$$

where Z is the canonical partition function and k_B is the Boltzmann constant. For two interacting species, the PMF, $W(\xi)$, is a function of the reaction coordinate ξ. The chosen reaction coordinate ξ is the distance between the geometric center of Fen and the clay surface, *i.e.*, the plane containing the basal oxygen, Ob. The whole set of Ob atoms forms the Mont

surface, noted surf hereafter. Increasing ξ should make possible to switch from Fen adsorbed on Mont to Fen desorbed. The PMF is the free energy profile of the system as a function of the separation distance ξ between Ca–Mont and Fen:

$$W(\xi) = -k_B T ln(g(\xi)) \tag{2}$$

where $g(\xi)$ is the distribution function of distances for the pair (Fen;Ca–Mont). Each biased dynamic simulation made possible to sample the configuration space around a value ξ_i of ξ by introducing into the Hamiltonian of the system for each simulation an harmonic potential V centered on the ξ_i value:

$$V = \frac{1}{2} k_i (\xi - \xi_i)^2 \tag{3}$$

The harmonic constant k_i is chosen to allow for an adequate sampling of the potential energy surface (PES). Table 2 gives the k_i values as well as the spacing of the umbrella windows, which are the two parameters to control the sampling of the PES.

Table 2: Parameters of the 11 biased MD trajectories: i is the window index, ξ_i is the value of the reaction coordinate around which the harmonic potential oscillated, k_i is the associated harmonic constant and t_i the duration of the simulation (ps).

i	ξ_i (Å)	k_i (kcal.mol^{-1}.Å^{-2})	t_i (ps)
1	4.41	14.3	20
2	4.70	28.6	20
3	4.89	114.3	13
4	5.05	14.3	20
5	5.55	57.1	12
6	5.58	114.3	13
7	5.65	114.3	16
8	5.78	57.1	25
9	6.20	57.1	14
10	6.40	14.3	11
11	7.11	14.3	13

The free energy surface was reconstructed from the distributions of ξ resulting from each biased MD simulation using the WHAM self-consistent method (weighted histogram approximation method)[63,64]. In addition, before plotting our free energy curves corresponding to

the Fen desorption from the surface, we checked if our sampling was sufficient. Indeed, we plotted the distribution functions of the reaction coordinate ξ and we were careful about their overlaps. These distributions are centered on the values of ξ around which the harmonic potentials of the umbrella sampling oscillate. We put Figure S1(i) in supplementary material that represents the plot of these different distributions as a function of ξ.

Results and discussion

When a pesticide is desorbed from the Ca–Mont surface, several mechanisms can be envisaged. First, the pesticide is desorbed and Ca^{2+} stays close to the surface (Figure 3(b)). Second, the pesticide and the interlayer cation are desorbed together (Figure 3(c)). In a last mechanism, we can envisage that PEST-Ca^{2+} complex moves away from the surface and finally, dissociates (Figure 3(d)). In the following, the simulated desorption profile is described and the Ca–surf distances are analyzed to determine, which is the desorption mechanism. Then, the hydration state of both cations helps to better understand the reaction path. Moreover, correlation between positions and hydration states of Ca^{2+} is highlighted.

Description of the desorption profile and Ca–surf distances

Figure 4 displays the calculated desorption profile of a fenhexamid molecule from the montmorillonite surface. The profile presents three free energy wells separated by two barriers of 2.5 and 5.0 kcal.mol^{-1}. The singularities of the free energy profile are noted P1, P2 and P3 for the minimums or wells and M1 and M2 for the maximums along the reaction coordinate ξ. We demonstrate in the Supporting Information that those maximums are transition states. For all the trajectories, Oe–Oe and Oe–Ob radial distribution functions (RDF) were plotted to confirm the liquid phase of water all along the desorption. On Figure S2, the Oe–Oe and Oe–Ob RDF are given for each singularity:

- Oe–Oe distances between the oxygen atoms of water molecules – For each singular-

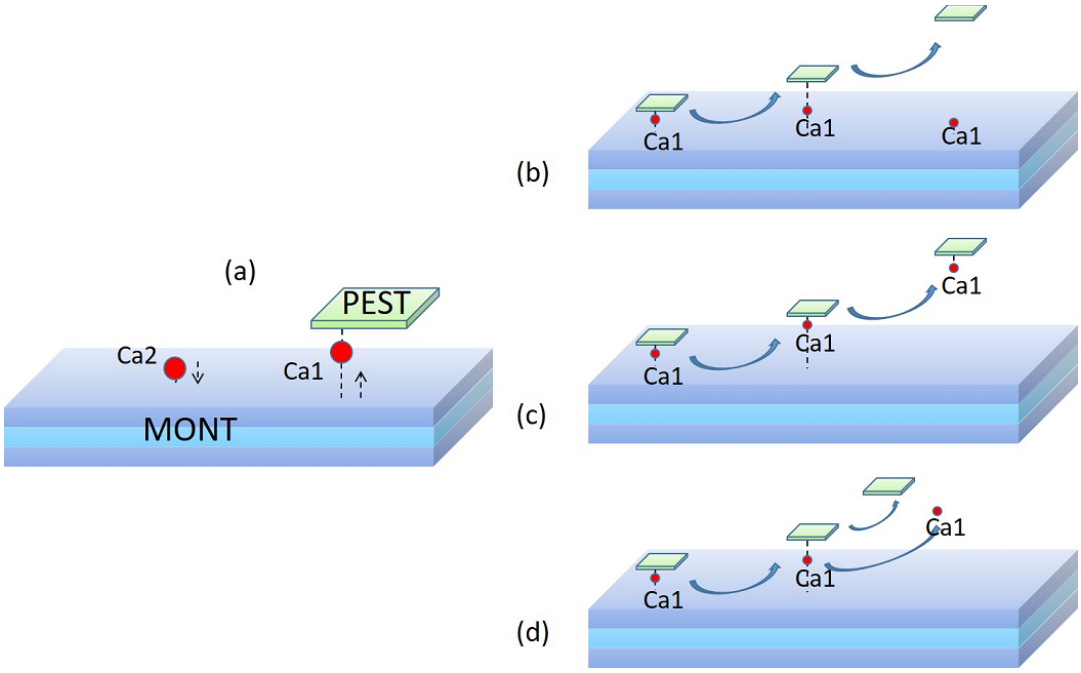

Figure 3: Mechanism propositions for the desorption of a pesticide (PEST) from a clay surface (MONT): (a) Definition of the Ca1 and Ca2 cations. Ca1 is the Ca^{2+} interacting with PEST and Ca2 does not interact with PEST; (b) PEST alone is desorbed from MONT, Ca1 remains attached to MONT; (c) PEST–Ca1 complex is desorbed from MONT; (d) PEST and Ca1 have a concerted departure from MONT but the interaction between PEST and Ca1 is not retained during the desorption.

ity, the profiles are almost stackable. In addition, the first peak of each distribution corresponds to a distance of ≈ 2.8 Å, which is characteristic of liquid water;

- Oe–Ob distances between the oxygen atoms of the water molecules Oe and the oxygen atoms of the surface Ob – Similarly, for each singularity, the distributions are comparable, which indicates a similar hydration of the surface all along the desorption. The first peak at ≈ 3.0 Å indicates that the water molecules are not in direct contact with the surface of the montmorillonite.

During the process, the global water structure does not seem to be affected by the desorption of Fen from Mont and the inevitable induced reorganizations.

In order to follow the movements of the cations during the desorption, we evaluated the distance distribution functions of both Ca^{2+} to the surface, denoted Ca1–surf and Ca2–

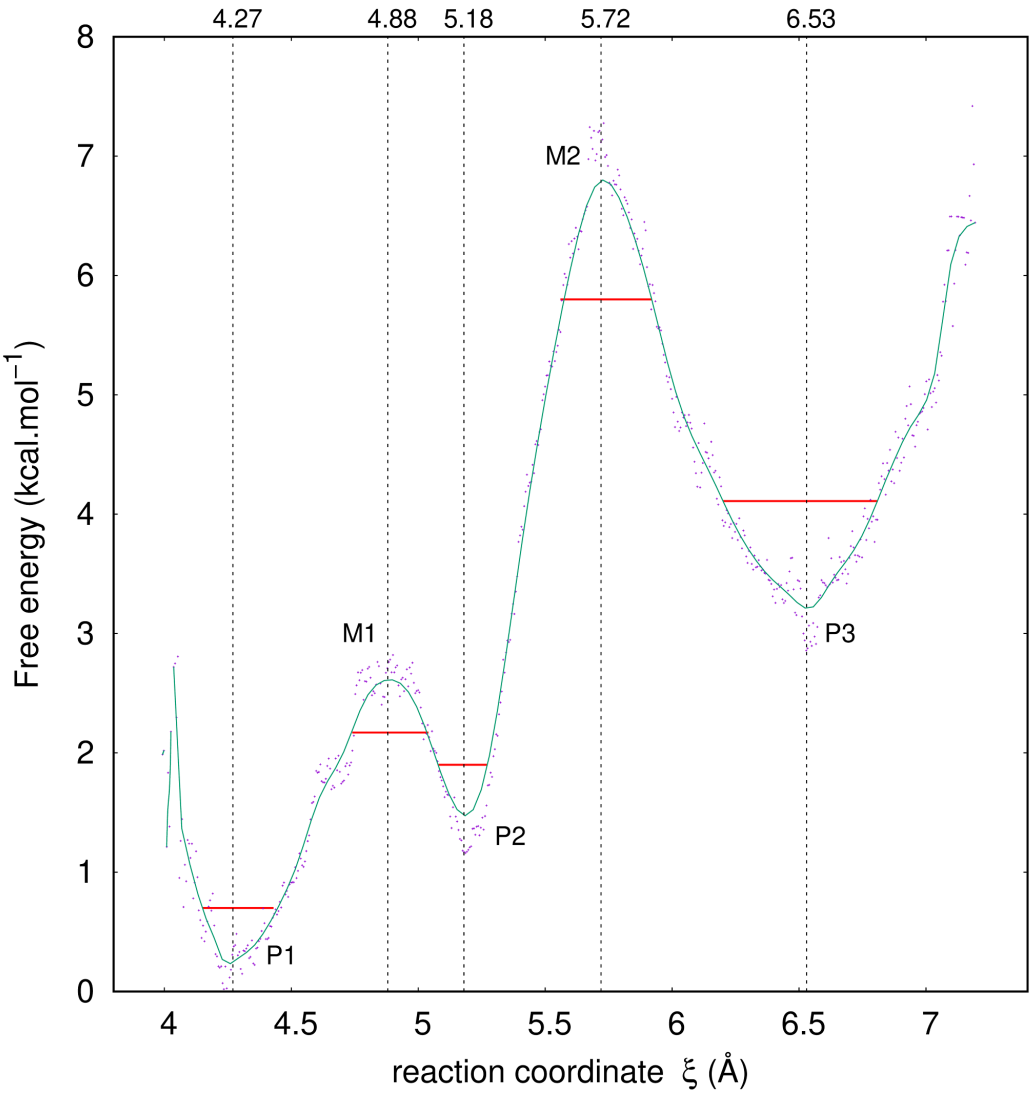

Figure 4: Free energy profile of fenhexamid desorption from the montmorillonite surface as a function of ξ, the distance from the geometric center of fenhexamid to surf, the surface containing the oxygen atoms Ob (see Figure 2). Every purple cross represents a structure visited during the 11 MD trajectories. The continuous green line gives the free energy profile of the desorption after smoothing. P1, P2, P3 are the minimums or energetic wells of this profile. M1 and M2 are the maximums. The zones delimited by the red horizontal lines enclose the structures considered as belonging to the minimums and to the maximums. Numbers on the top of the graph are the ξ values for each singularity.

surf thereafter (see Figure S3). Within P1, Ca1 is close to the surface and the Ca1–surf distribution has a double peak with two maximums at $\approx$ 1.1 Å and $\approx$ 1.6 Å (see Figure S3(a)). Ca2 is further from Mont with three preferred positions $\approx$ 2.7, 4.1 and 5.2 Å. For P2, the Ca1–surf distribution displays a single peak centered at 2.3 Å, while the distribution

of Ca2–surf has a peak centered at 2.5 Å. For P3, the distributions share common features with P1. The Ca1–surf distribution has only one maximum at 1.4 Å, as for Ca2, two preferred positions $\approx$ 2.5 and 4.0 Å exist. These observations show that the simulated mechanism is the one shown in Figure 3(b). In P1 and P2, Ca1 interacts with Fen whereas, in P3, the Fen–Ca1 interaction is broken and Ca1 comes back closer to the surface.

Hydration state of the cations

In the analysis of the desorption free energy profile of Fen from the montmorillonite surface, the hydration states of both Ca^{2+} are important to explain the process. Thus, the arrangement of both Ca^{2+} first HS is investigated in the following.

On Figure S4, the Ca–Oe RDF have been extracted from the trajectories and sorted by singularities of the free energy profile: i) for Ca1–Oe, all the profiles are similar, with a first peak centered on 2.3 Å and the Ca1–Oe RDF first minimum equals zero at 3.0 Å; ii) for Ca2–Oe, all the curves are also similar, the first peak is more intense but also centered on 2.3 Å and the Ca2–Oe RDF first minimum also equals zero at 3.0 Å. Thus, a water molecule has been counted in the first HS of a calcium cation when $d_{Ca-Oe} \leq 3.0$ Å.

Then, to better understand the shape of the distributions of Figure S3, we sorted the structures according to the number of water molecules in the first HS (see Figures 5 for wells and 6 for maximums). For both cations Ca1 and Ca2, we were able to deconvolute the peaks of Ca–surf distributions and to draw the following information:

- Ca1 is hydrated by 1 to 4 water molecules: 1 to 2 for the structures in P1, 2 to 3 for M1 and P2 and 2 to 4 (with a majority of 3 water molecules around Ca1) for M2 and P3. Moreover on average, Ca1–surf distances are similar for P1 and P3 ($\approx$ 1.4 Å). For M1, P2 and M2, this average distance is longer, $\approx$ 2.4 Å, because Ca1 interacts with Fen, which moves away from the surface. For the majority of these structures, three water molecules solvate Ca1.

- Ca2 is solvated by 5 to 8 water molecules: 5 to 8 for P1, 5 for M1, 5 (to 6) for P2 and M2, and 5 to 7 for P3. In M1 and P2, Ca2 is localized at an average distance of about 2.5 Å from Mont with an inner first HS, thus including the surface in a square-based bi-pyramid structure. This kind of structures with 5 water molecules in the first HS is predominant in M2 (Ca2–surf distance $\approx$ 2.5 Å) but Ca2 can also be solvated by 6 water molecules (Ca2–surf distance $\approx$ 3.9 Å). In P1 and P3, more hydration states are accessible to Ca2, while Ca1 is located near the surface ($\approx$ 1.4 Å). In P1 and P3, Ca2 displays different HS: a square-based pyramid (5 H_2O), an octahedron (6 H_2O), and a distorted square antiprism (8 H_2O) (both the latest are among the most stable of the first HS of Ca^{2+} according to the literature). In the interlayer space of an hydrated montmorillonite system, Holmboe and coworkers showed that the 5W hydration state allows full hydration of Ca^{2+} cations[17,18]. For Holmboe at 300 K, full hydration for Ca^{2+} includes 8 water molecules in the first HS, whereas, Fockenberg *et al.* counts 6 water molecules in the first HS of Ca^{2+} in aqueous solution[22]. Our results are consistent with those obtained by Holmboe *et al.* and Fockenberg *et al.* but in our simulations, a great amount of structures in P1, P2 and P3 count 5 and 7 water molecules in the first HS of Ca^{2+}.

Finally, comparing Ca1–surf and Ca2–surf distances in P1, P2 and P3, we can see that, when Ca1 is close to the surface ($\approx$ 1.4 Å) then Ca2 is further ($\approx$ 4.0 Å) (in P1 and P3), whereas if Ca1–surf equals about $2.3 - 2.5$ Å then Ca2–surf is in the same range (in P2). Everything happens as if Ca1–surf and Ca2–surf are correlated with each other. In the following part, we then investigate whether there is a correlation between the distances of the two cations to the surface and we seek to relate this to the hydration of the cations.

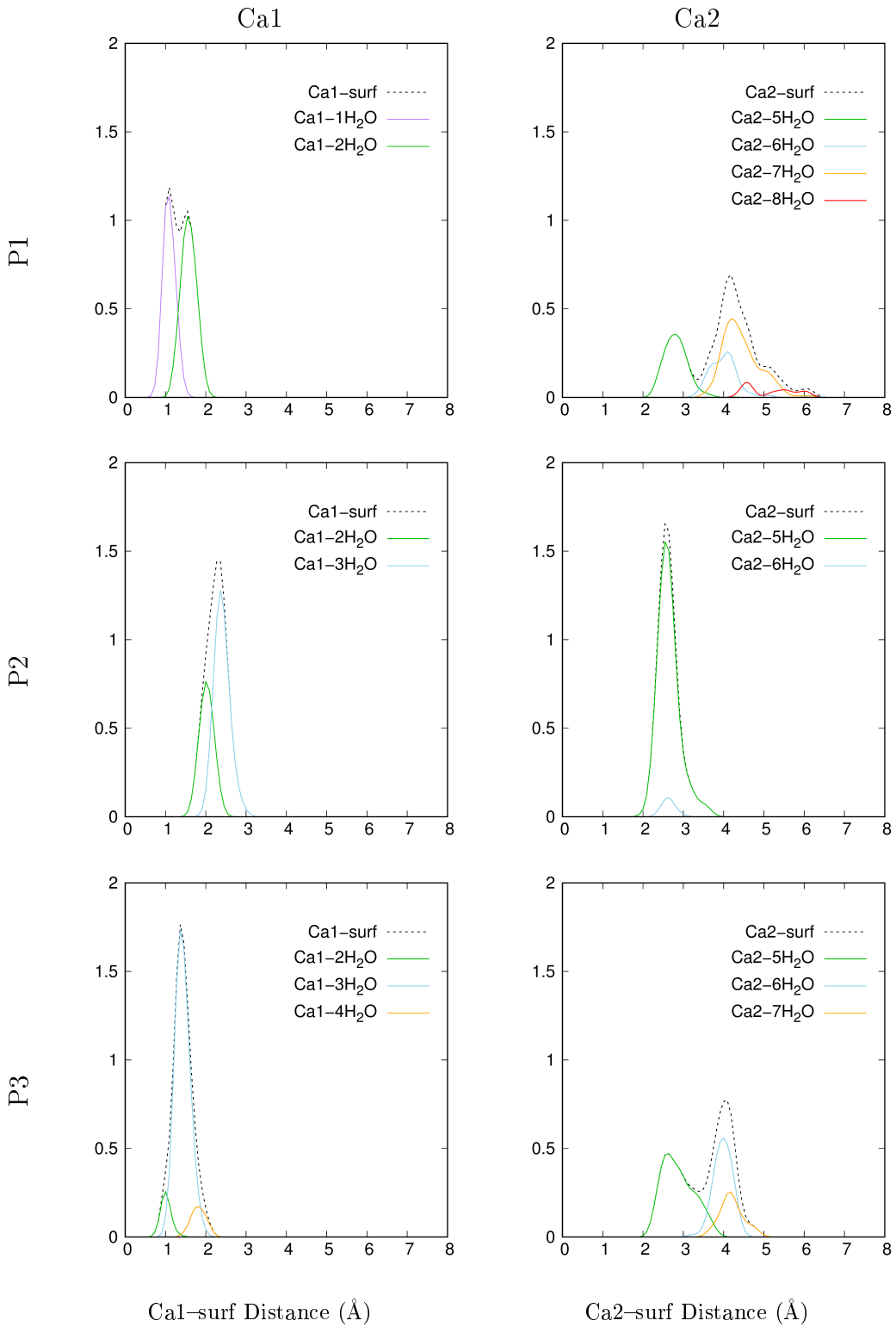

Figure 5: Ca1–surf and Ca2–surf normalized distributions for each of the wells P1, P2 and P3 of the free energy profile. In each well, the structures were sorted according to the number of water molecules in the first HS ($d_{Oe-Ca} \leq 3.0$ Å) of Ca1 or Ca2.

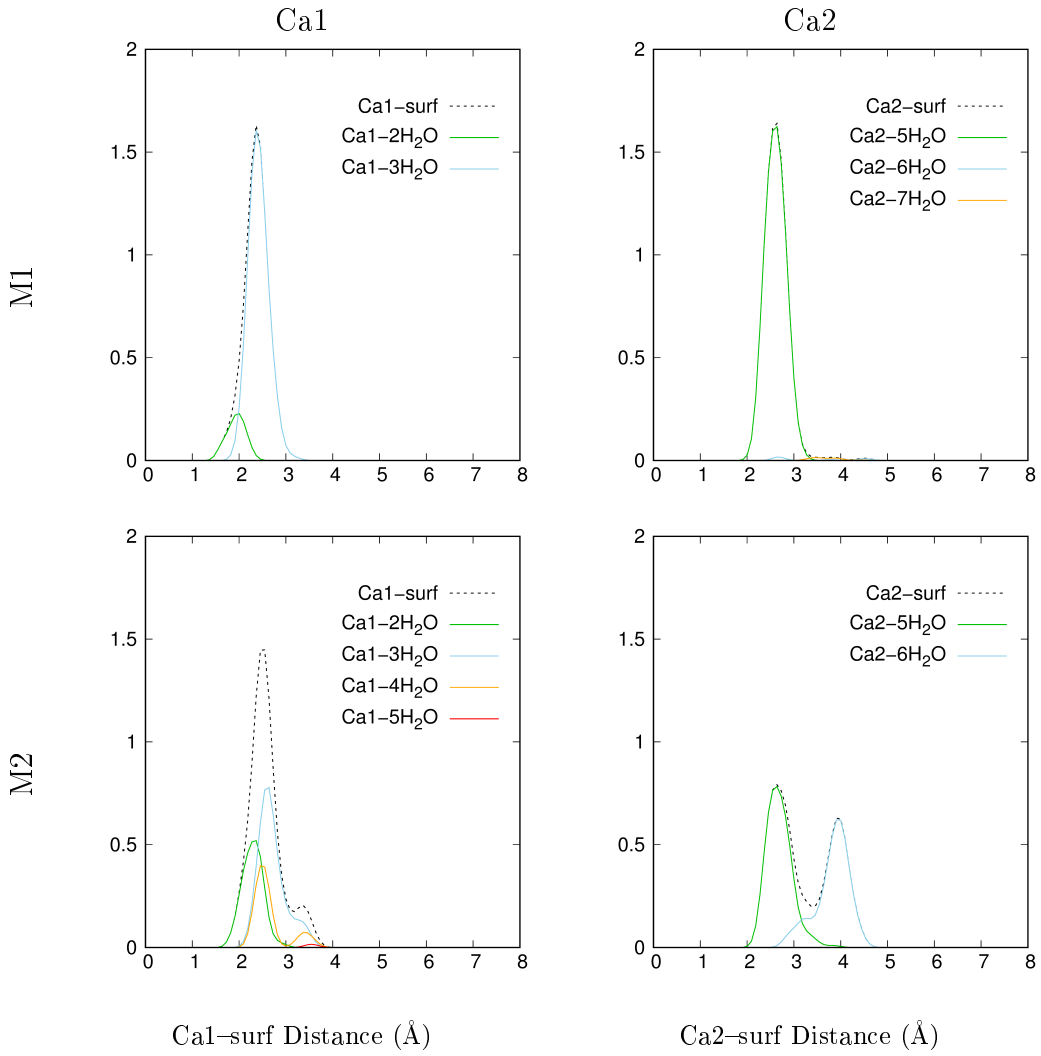

Figure 6: Ca1–surf and Ca2–surf normalized distributions for each of the maximums M1 and M2 of the free energy profile. For each maximum, the structures were sorted according to the number of water molecules in the first HS ($d_{Oe-Ca} \leq 3.0$ Å) of Ca1 or Ca2.

Correlation between positions and hydration states of both cations

Figures 7 and 8 report the density of structures regarding to Ca1–surf and Ca2-surf values visited for the minimums (Figure 7) and the maximums (Figure 8) of the free energy desorption profile. Moreover, Figure 9 reports four snapshots of structures along the free energy profile of desorption of Fen from Mont: one for each minimum and one for the M2 maximum, which differs from other singularities. The number of water molecules in the first HS of Ca1 and Ca2 is given as well as the Ca1–Ca2, Ca1–surf, Ca2–surf and Ca1–Om distances (Om is the oxygen atom of the Fen carbonyl group).

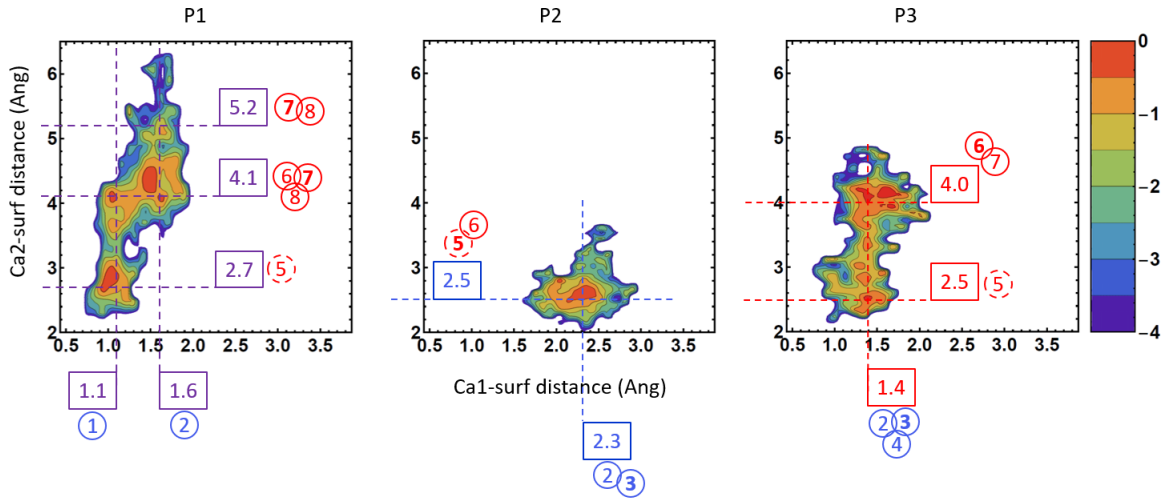

Figure 7: Density of structures for the three wells P1, P2 and P3 of Fen desorption from the montmorillonite, at given Ca1–surf and Ca2–surf distances. Distances are in Å, the logarithm (*log*) of the density of structures is represented (scale from -4 to 0). In round boxes, the numbers of water molecules in the first HS around Ca1 (blue) and Ca2 (red) are also given (in bold: the most abundant; in dashed circles: first HS including the surface, square-based bi-pyramid structures formed by 5 water molecules and the surface). In square boxes, distances corresponding to the maximums of density of structures are put forward.

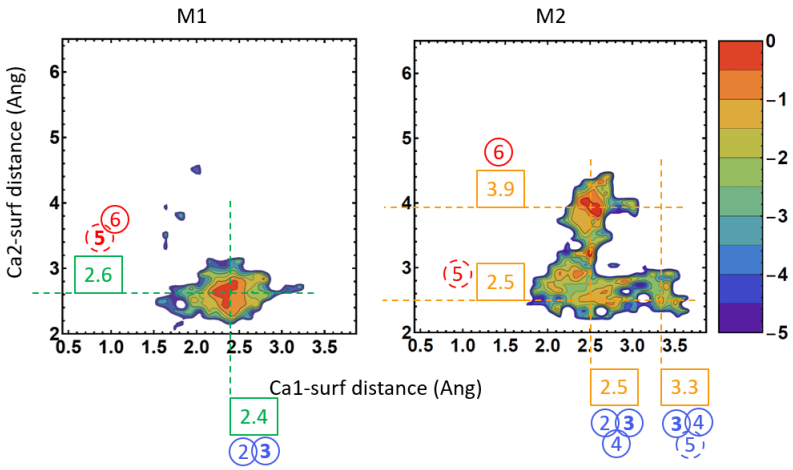

Figure 8: Density of structures for both minimums M1 and M2 of Fen desorption from the montmorillonite, at given Ca1–surf and Ca2–surf distances. Distances are in Å, the logarithm (*log*) of the density of structures is represented (scale from -5 to 0). In round boxes, the numbers of water molecules in the first HS around Ca1 (blue) and Ca2 (red) are also given (in bold: the most abundant; in dashed circles: first HS including the surface, square-based bi-pyramid structures formed by 5 water molecules and the surface). In square boxes, distances corresponding to the maximums of density of structures are put forward.

Snapshot	M2
	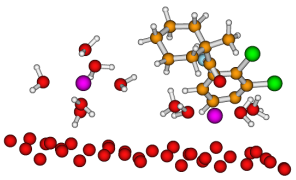
HS_{Ca1}	4
HS_{Ca2}	6
Ca1–Ca2	8.34
Ca1–surf	2.57
Ca2–surf	4.03
Ca1–Om	2.15

Snapshots	P1	P2	P3
	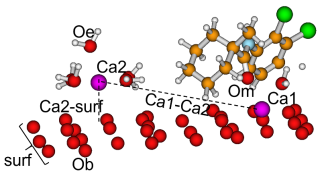	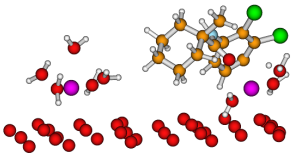	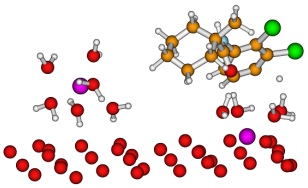
HS_{Ca1}	1	3	4
HS_{Ca2}	5	5	6
Ca1–Ca2	10.48	11.21	10.60
Ca1–surf	1.12	2.52	1.44
Ca2–surf	2.80	2.66	4.17
Ca1–Om	2.36	2.25	4.02

Figure 9: Snapshots taken in the 3 minimums, P1, P2 and P3, and in the M2 maximum of the free energy profile of desorption of Fen from Mont. For clarity, only the Ob oxygen atoms are represented for the Mont surface. For the same reason, only the water molecules involved into the first HS of Ca1 and Ca2 are represented ($d_{Oe-Ca} \leq 3.0$ Å). HS_{Ca1} and HS_{Ca2} are the numbers of water molecules in the first HS of Ca1 and Ca2, respectively. Ca1–Ca2, Ca1–surf, Ca2–surf and Ca1–Om distances are given in Å. Om is the oxygen atom of the Fen carbonyl group.

For P1, the density of structures presents four high density basins (B):

B1. Ca1–surf ≈ 1.1 Å and Ca2–surf ≈ 2.7 Å: Ca1 is solvated by only one water molecule and Ca2 by 5;

B2. Ca1–surf ≈ 1.1 Å and Ca2–surf ≈ 4.1 Å: Ca1 is solvated by only one water molecule and Ca2 mostly by 7;

B3. Ca1–surf ≈ 1.6 Å and Ca2–surf ≈ 4.1 Å: Ca1 is solvated by two water molecules and Ca2 by 6 or 7, mostly by 6;

B4. Ca1–surf ≈ 1.6 Å and Ca2–surf ≈ 5.2 Å: Ca1 is solvated by two water molecules and Ca2 by 7 or 8.

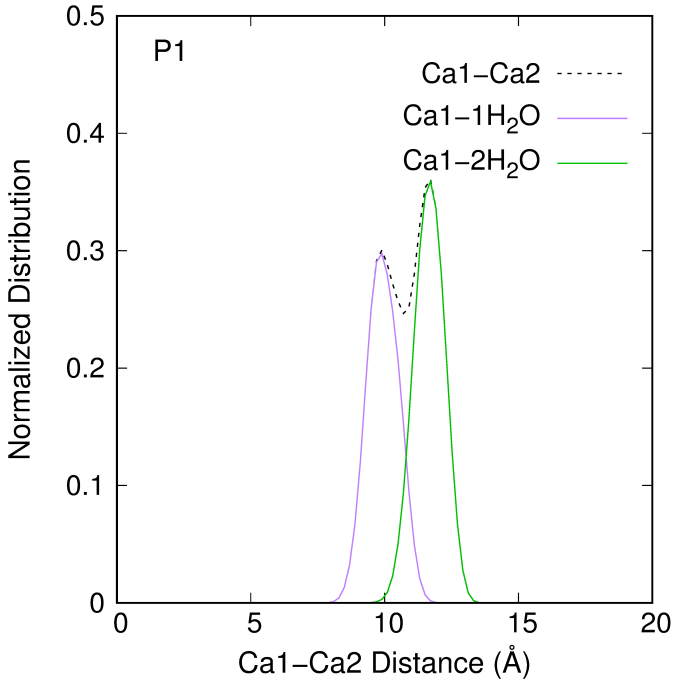

Figure 10: Ca1–Ca2 normalized distribution for the first minimum P1 of the free energy profile. The structures were sorted according to the number of water molecules in the first HS ($d_{Oe-Ca} \leq 3.0$ Å) of Ca1.

Ca1–surf and Ca2–surf distances increase with the number of water molecules into their first HS. One may wonder why no structure corresponding to the couple Ca1–surf ≈ 1.6 Å and

Ca2–surf ≈ 2.7 Å, *i.e.* Ca1 solvated by 2 water molecules and Ca2 by 5, has been found. For the structures corresponding to B1, Ca1–Ca2 distances are shorter in average (see Figure 10) than in dry Mont (d_{Ca-Ca} = 10.341 Å). But in the hypothetical situation, Ca1–surf ≈ 1.6 Å and Ca2–surf ≈ 2.7 Å (Ca1 solvated by 2 water molecules and Ca2 by 5) compared to B1, Ca1 moves away from the surface, while Ca2 stands still resulting in the shortening of the Ca1–Ca2 distance. The cation charge repulsion is no longer compensated by the surface and not yet by water molecule screening. Thus, when Ca1 moves away from the surface, Ca2 has to do the same (B3 and B4). Thus, Ca1–Ca2 distances become longer in average (see Figure 10) than in dry Mont and Ca2 first HS grows to 6 till 8 water molecules. In B2, Ca1 solvated by one water molecule stays close to Mont and Ca2 is further from the surface. In this case, Ca1–Ca2 distances are shorter than in dry Mont, which is probably possible thanks to the screening of Ca2 by the higher number of water molecules into its first HS (6 to 8 but mostly 7). Experimental evidence allows to list two different types of interaction of water with the cations of the clay: i) water molecules bound to the cations attached to the clay surface (inner HS); ii) water molecules bound to fully hydrated cations detached from the surface (outer HS). Snapshot P1 belongs to B1 and presents 5 water molecules around Ca2 and a Ca2–surf distance of 2.80 Å (see Figure 9). Thus, the Ca2 inner HS is a square-based bi-pyramid structures formed by 5 water molecules and the surface. Ca1 stays attached to the surface and to Fen by the monodentate complexation site Om. Thus, only one water molecule enter the space between Fen and the surface near Ca1 to form its first HS.

On Figure 7 P2, the density of structures shows only one basin with an high density of structures corresponding to Ca1–surf ≈ 2.3 Å and Ca2–surf ≈ 2.5 Å. Ca1 is solvated by two but predominantly three water molecules and Ca2 by mostly 5. Localization of the density goes along with Ca1–Ca2 distances around 10 Å comparable with dry Mont. Compared to P1, Ca1 positions are further from the surface and Ca1 are at almost equal distances to Mont than Ca2. For the second minimum, the snapshot P2 shows again 5 water molecules around Ca2 and an even shorter Ca2–surf distance than in P1 (2.66 Å, see Figure 9). The

Ca2 inner HS is a square-based bi-pyramid structure formed by 5 water molecules and the surface. Here, Ca1 is still attached to the surface and to Fen (Ca1–Om = 2.25 Å). As Fen moves away from the surface from P1 to P2, a second and a third water molecules enter the space between Fen and the surface near Ca1. Its HS contains 3 water molecules.

For P3, Ca1 is closer to the surface, while the interaction between Ca1 and the oxygen atom of Fen carbonyl group is lost. The structures present Ca1–surf distances around 1.4 Å corresponding to mostly three water molecules in the first HS. These water molecules insert the space between Fen and Ca1. Again as in P2, Ca1–Ca2 distances are in average roughly equal to the Ca–Ca distance in dry Mont. If the first HS of Ca2 counts 5 water molecules, thus Ca2–surf is about 2.5 Å, while if the first HS of Ca2 counts 6 to 7 water molecules, thus Ca2–surf is longer being around 4.0 Å. In the P3 minimum, while Fen moves away from the surface,the space between Fen and the surface can host additional water molecules. In snapshot P3, we chose to show on Figure 9, a structure for which, Ca2 has 6 apices and Ca1 has 5. For Ca2, 6 water molecules are at the apices of a square-based bi-pyramid. For Ca1, 4 water molecules and the surface constitute the five apices of a square-based pyramid. Ca2 is located at the center of an outer HS whereas Ca1 is at the center of an inner HS.

On Figure 8, for M1 and M2 maximums, the density of structures according to both distances Ca1–surf and Ca2–surf are given. For M1 transition state (see Figure S6(a)), the density is localized around Ca1–surf = 2.4 Å and Ca2-surf = 2.6 Å. HS_{Ca1} contains mostly 3 water molecules and HS_{Ca2} 5. This graph is quite similar to P2 graph on Figure 7. Thus M1 resembles the well, which is downstream and could be qualified of a late connecting maximum. On the other hand, M2 graph connecting P2 and P3 looks like the P2 well, which is upstream, for the basin around Ca1–surf = 2.5 Å and Ca2–surf = 2.5 Å (noted B'1). As well as for P2, in B'1, HS_{Ca1} is mostly 3 and HS_{Ca2} = 5. However, new basins are visited:

B'2. Ca1–surf = 2.5 Å and Ca2–surf = 3.9 Å, HS_{Ca1} contains two to four but mostly 3 water molecules and HS_{Ca2} contains mostly 6 water molecules;

B'3. Ca1–surf = 3.3 Å and Ca2–surf = 2.5 Å, HS_{Ca1} contains three to five but mostly 3 water molecules and HS_{Ca2} contains mostly 5 water molecules.

On Figure 9, snapshot M2 belonging to B'2 shows a structure for which, both Ca^{2+} cations are in a 6 apices HS (see Figure 9). For Ca2, 6 water molecules are at the apices of a square-based bi-pyramid. For Ca1, 4 water molecules, Om and the surface constitute the apices of a square-based bi-pyramid again. Ca2 is located at the center of an outer HS whereas Ca1 is at the center of an inner HS.

Alternative desorption mechanisms

In the previously presented desorption profile, the interaction between Ca1 and Fen is lost in P3 in agreement with the mechanism shown on Figure 3(b). To confirm this mechanism is preferred or not, an alternative mechanism has been studied. When the chosen reaction coordinate ξ increases beyond 5.7 Å (M2), all the structures end up in well P3 with Ca1-surf distances around 1.4 Å. Thus, one question arises: is it possible that Fen desorbed from Mont along with Ca1 (Figure 3(c))? If so, is this mechanism energetically accessible? For the structures of B'3 (Figure 8 M2), Ca1 is moving away from the surface (Ca1–surf = 3.3 Å). The interaction between Ca1 and the surface is lost but the monodentate interaction between Fen and Ca1 via Om is preserved. Thus, ξ is adapted to deal with the desorption of Fen–Ca1 complex from the surface (see Figure 3(c)). We decided to take over from a B'3 structure and with the same reaction coordinate ξ to launch 6 new biased MD trajectories (see windows 9 to 14 on Table 3 and overlapping distributions of the umbrella sampling simulations on Figure S1(ii)). Therefore, we obtained a new end of profile for $\xi > 5.8$ Å that we superimposed to the first in Figure 11. This new profile corresponds to the desorption of the Fen–Ca1 complex from the surface (Figure 3(c)). After M2, the new profile differs from the previous one with a minimum P3c at $\xi = 6.23$ Å and a maximum M3c for $\xi = 6.74$ Å. The new profile is energetically disfavored with respect to the previous one. The bottoms of the wells P3 and P3c are ≈ 2 kcal/mol apart in free energy and offset by 0.3 Å. In P3c, the

Table 3: Parameters of the 14 biased MD trajectories: i is the window index, ξ_i is the value of the reaction coordinate around which the harmonic potential oscillated, k_i is the associated harmonic constant and t_i the duration of the simulation (ps). In bold, the characteristic of the 6 trajectories that differ from the first energy profile are given.

i	ξ_i (Å)	k_i (kcal.mol^{-1}.Å^{-2})	t_i (ps)
1	4.41	14.3	20
2	4.70	28.6	20
3	4.89	114.3	13
4	5.05	14.3	20
5	5.55	57.1	12
6	5.58	114.3	13
7	5.65	114.3	16
8	5.78	57.1	25
9	**6.20**	**57.1**	**12**
10	**6.40**	**14.3**	**12**
11	**7.11**	**114.3**	**12**
12	**7.11**	**114.3**	**12**
13	**7.11**	**114.3**	**12**
14	**7.11**	**14.3**	**12**

Om–Ca1 interaction is present. Ca1 is further from the surface than in P3 as it can be seen in Figure 12 (2.6 and 1.4 Å respectively). Moreover, one more water molecule forms the first HS in P3c ($HS_{Ca1} = 4$ mostly) than in P3 ($HS_{Ca1} = 3$ mostly). Concomitantly, the main difference on Ca2 HS is the loss of the structures with 5 water molecules in HS_{Ca2} in favor of $HS_{Ca2} = 6$. The M3c maximum of the new profile is ≈ 2.5 kcal/mol higher in energy than P3c. Ca1 in those structures is hydrated mostly by 5 water molecules and is, in average, distant of ≈ 3.5 Å from the surface; Om being the sixth apex of the Ca1 octahedron. Ca2 remains mainly in the same hydration pattern than in P3c ($HS_{Ca2} = 6$).

After M2 transition state (see Figure S6(b)), either the (b) path is followed losing the Ca1–Fen interaction or the (c) path, higher in energy, keeping this interaction. Choosing a path, (b) or (c), is exclusive. In order to understand why we obtained two distinct mechanisms, we conducted an other profile (see Figure 13). Starting from a P3 structure (Ca1 close to the surface and Fen–Mont ≈ 6.5 Å), we defined a new reaction coordinate $\xi' =$ Ca1–surf. When ξ' lengthens, Ca1 is going away from the surface and is getting closer to Fen. The reaction

profile shows two minimums, PI and PII, and one maximum, MI. PI bottom of the well is less than 1 kcal/mol lower in free energy than PII. The barrier from PI is about 6 kcal/mol, which is consistent with the exclusivity of the paths. In Figure S5, Ca1–surf and Ca2–surf normalized distributions for each of the PI, PII and MI singularities are presented. For the first HS of Ca1, PI is in accordance with the P3 well of path (b). However, for all structures in PI, $\mathrm{HS}_{Ca1} = 3$ because the Ca1–surf distance is in between 1.225 and 1.485 Å excluding $\mathrm{HS}_{Ca1} = 2$ and $\mathrm{HS}_{Ca1} = 4$ structures. Similarly, PII is consistent with P3c (path(c)) with mostly 4 water molecules in the Ca1 first HS. Going from PI to PII via MI, an increase in HS_{Ca1} is observed from 3 to 5. Ca2, the non interacting cation, has an HS of mostly 6 or 7 water molecules.

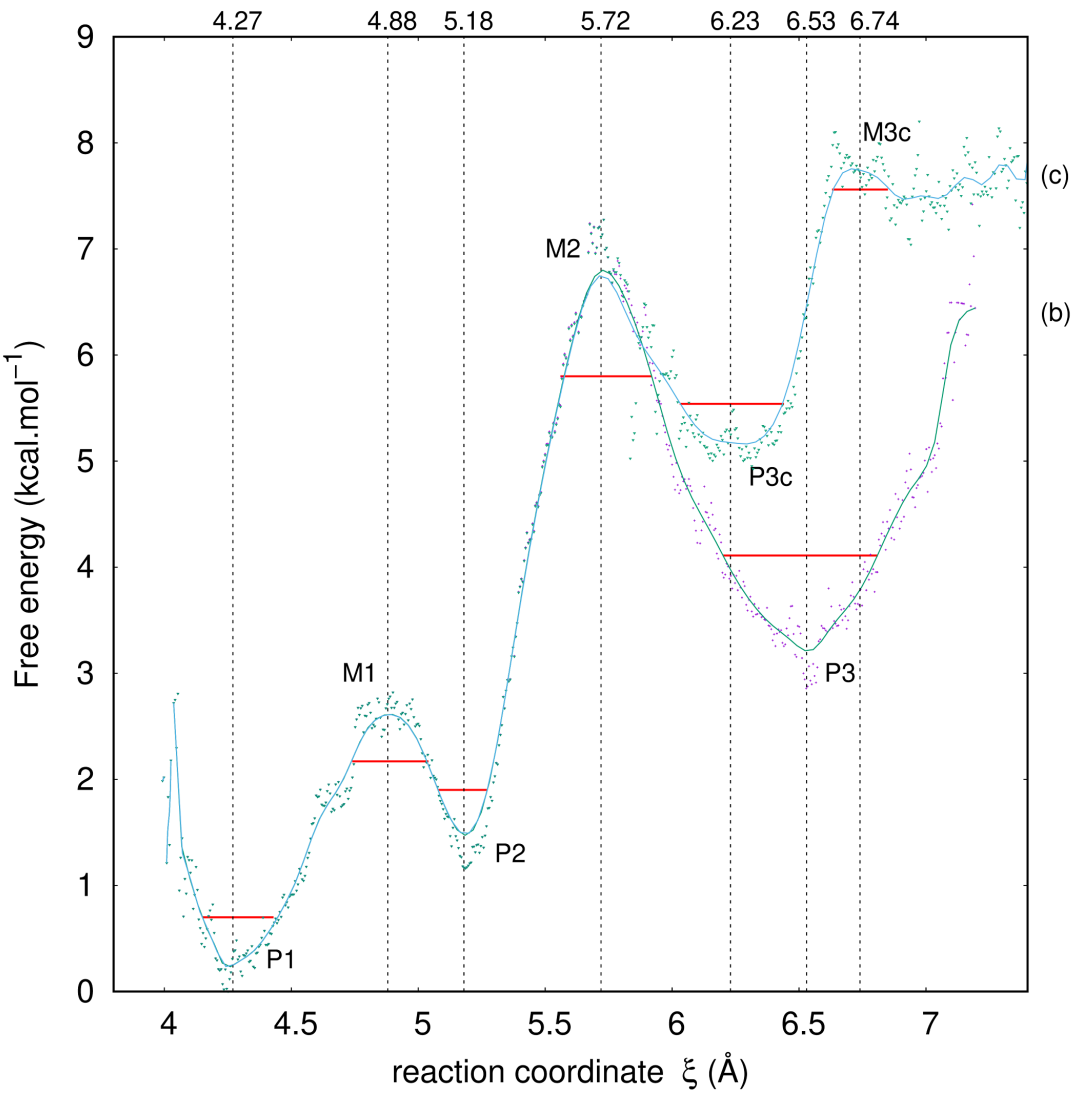

Figure 11: Free energy profile of fenhexamid desorption from the montmorillonite surface as a function of ξ, the distance from the geometric center of fenhexamid to surf, the surface containing the oxygen atoms Ob (see Figure 2). Every purple or green cross represents a structure visited during the 11 (b) and 14 (c) MD simulations. The continuous green line gives the free energy profile of the desorption after smoothing. P1, P2, P3 and P3c are the minimums or energetic wells of this profile. M1, M2 and M3c are the maximums. The zones delimited by the red horizontal lines enclose the structures considered as belonging to the minimums and to the maximums. Numbers on the top of the graph are the ξ values for each singularity.

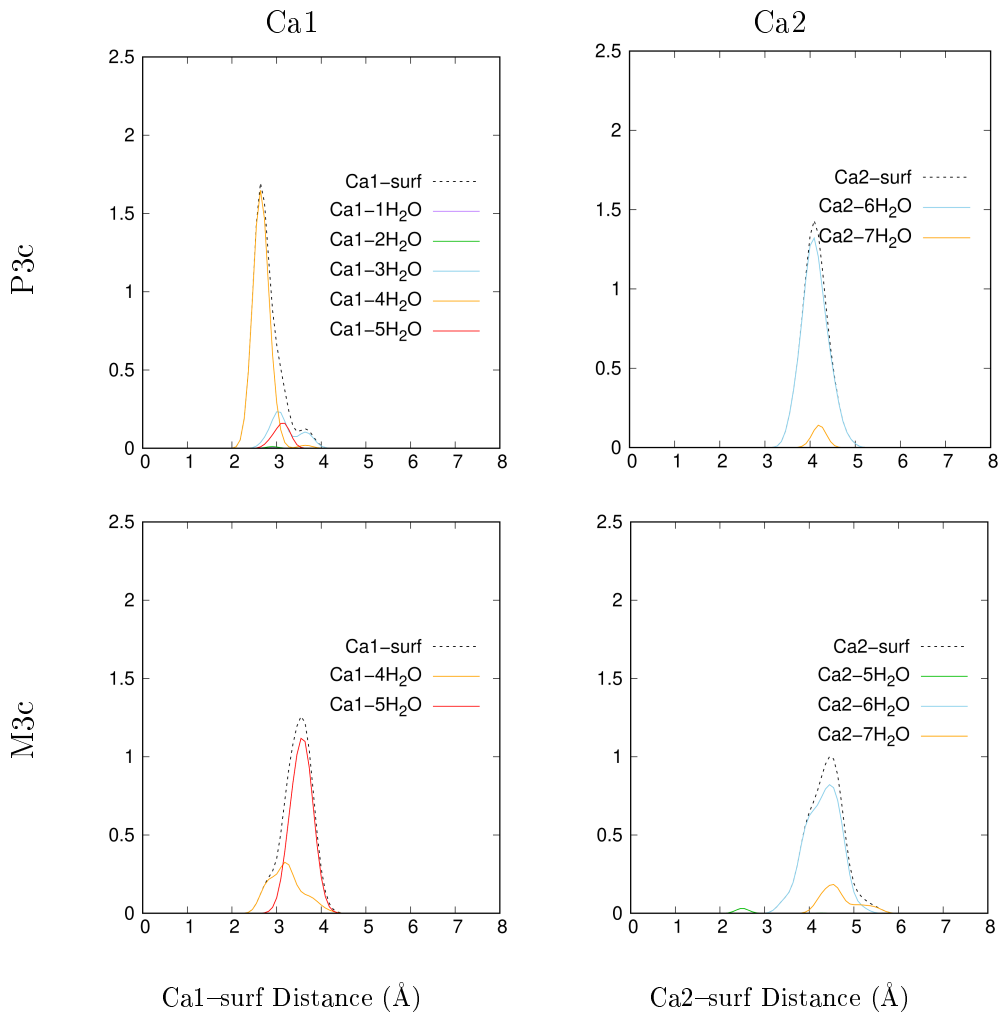

Figure 12: Ca1–surf and Ca2–surf normalized distributions for the P3c well and the M3c maximum of the free energy profile. In P3c and M3c, the structures were sorted according to the number of water molecules in the first HS ($d_{Oe-Ca} \leq 3.0$ Å) of Ca1 or Ca2.

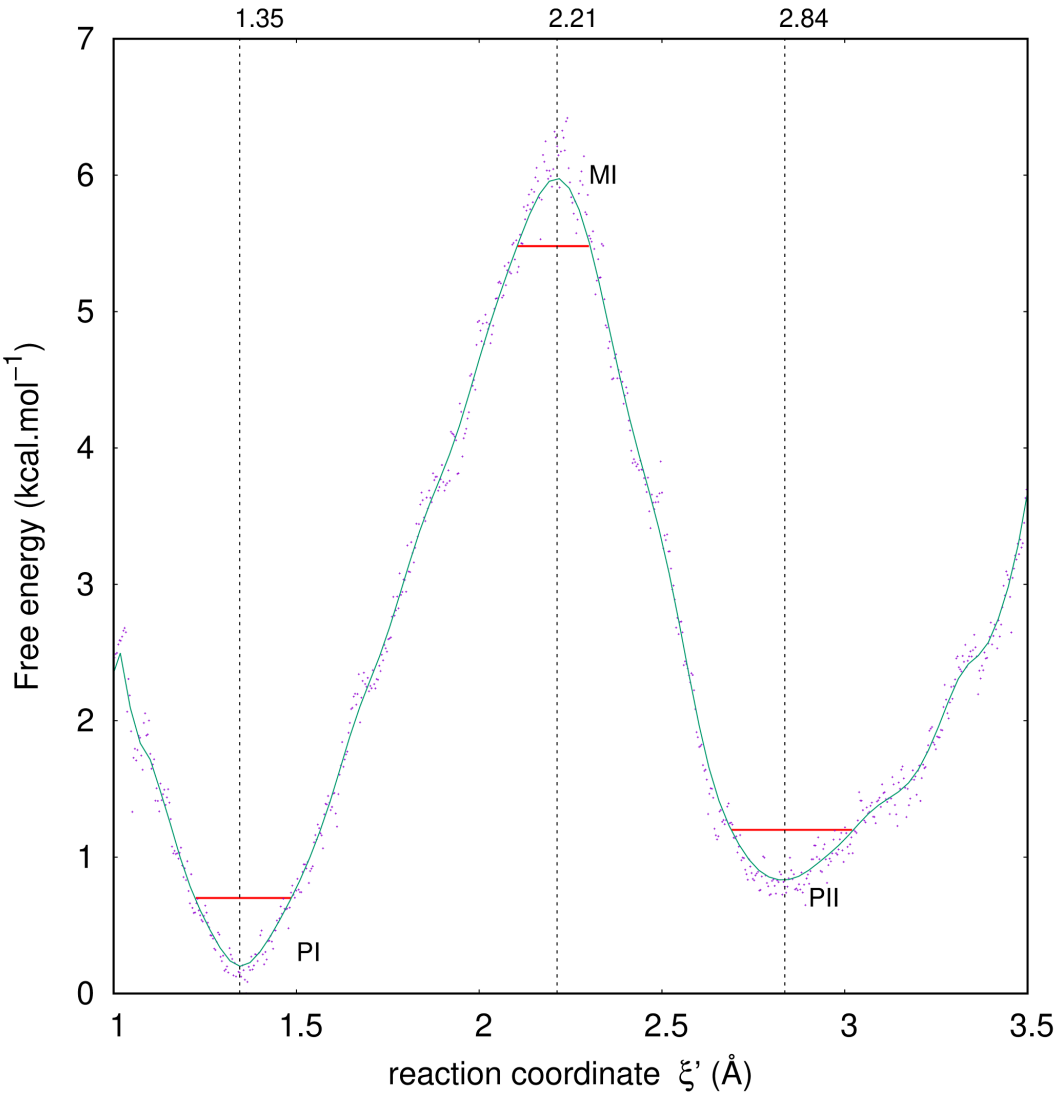

Figure 13: Free energy profile of Ca1 moving away from the surface. ξ' is the distance between Ca1 and surf, the surface containing the oxygen atoms Ob (see Figure 2). Every purple cross represents a structure visited during the MD simulations. The continuous green line gives the free energy profile after smoothing. PI and PII are the minimums or energetic wells of this profile. MI is the maximum. The zones delimited by the red horizontal lines enclose the structures considered as belonging to the minimums and to the maximums. Numbers on the top of the graph are the ξ' values for each singularity.

Conclusion

The desorption of fenhexamid from an hydrated Ca–montmorillonite surface has been studied by *ab initio* molecular dynamics. The free energy profile is common to both mechanisms considered until the fenhexamid reaches a distance of about 5.7 Å from the surface. Initially, the fenhexamid is close to the surface and in interaction with the Ca1 cation. At the passage of the first barrier, an additional water molecule joins the first HS of Ca1 passing from 1 to 2 molecules to 2 to 3. The associated free energy barrier is 2.5 kcal/mol. Thereafter, a second barrier (5 kcal/mol) is crossed corresponding to an increase in the hydration of Ca1: 2 to 4 water molecules for M2 (see Figure 11). After M2, two pathways are possible: the fenhexamid is desorbed, it disassociates from Ca1, which then interacts with the surface (Figure 3(b)); the Fen–Ca1 complex is desorbed from Mont (Figure 3(c)). The profile corresponding to (b) mechanism is preferred: the bottoms of wells P3 and P3c are distant by 2 kcal/mol in free energy. From M2 to P3 (b), the first HS of Ca1 contains predominantly 3 water molecules while for structures belonging to P3c (c), the preferred hydration is 4. Following the (c) mechanism, a new barrier (P3c→M3c) is encountered (2.5 kcal/mol) corresponding to the addition of an extra water molecule in Ca1 first HS, *i.e.*, 5 water molecules in majority. This work shows that once one pathway is taken the other is no longer accessible except by crossing a free energy barrier of more than 5 kcal/mol (see Figure 13). By pursuing (c) pathway beyond M3c, the Fen–Ca1 complex could evolve towards dissociation to increase the hydration energy of each entity: Ca1 and Fen. This pathway is evoked in Figure 3 as (d) mechanism. However, the (b) desorption mechanism will remain preferred.

Acknowledgement

This work was granted access to the HPC resources of CALMIP supercomputing center under the allocation 2018-[P1222] and of CINES under the allocation 2018-[cpq7002] made by GENCI.

This work was carried out using the open-source, community-developed PLUMED library [1], version 2.x [2] (or alternatively version 1.x [3]).

Supporting Information Available

The following files are available free of charge.

- Figure S1: Overlapping distributions of ξ, the distance from the geometric center of fenhexamid to surf, obtained for the umbrella sampling simulations to determine the free energy profile of fenhexamid desorption from the montmorillonite surface: (i) mechanism (b); (ii) mechanism (c) (see Figure 3).
- Figure S2: Oe–Oe (a) and Oe–Ob (b) radial distribution functions for the singularities P1, M1, P2, M2 and P3 of the free energy profile of desorption of Fen from Mont. Oe are the oxygen atoms of water molecules and Ob, the surface oxygen atoms.
- Figure S3: Ca1–surf (a) and Ca2–surf (b) normalized distributions for the singularities P1, M1, P2, M2 and P3 of the free energy profile of desorption of Fen from Mont.
- Figure S4: Ca1–Oe (a) and Ca2–Oe (b) radial distribution functions for of the singularities P1, M1, P2, M2 and P3 of the free energy profile of desorption of Fen from Mont. Oe are the oxygen atoms of water molecules. Ca1 and Ca2 are the Ca^{2+} cations in the computational cell. Ca1 is in interaction with Fen.
- Figure S5: Ca1–surf and Ca2–surf normalized distributions for each of the maximums PI and PII and for the MI well of the free energy profile of Ca1 moving away from the surface. For each maximum, the structures were sorted according to the number of water molecules in the first HS ($d_{Oe-Ca} \leq 3.0$ Å) of Ca1 or Ca2.
- Figure S6: Distributions of ξ, the distance from the geometric center of fenhexamid to surf, obtained for simulations starting: (a) from 7 TS configurations for the M1 transition state; (b) from 7 TS configurations for the M2 transition state.

References

(1) Bessac, F.; Hoyau, S. Pesticide interaction with environmentally important cations: A theoretical study of atrazine. *Computational and Theoretical Chemistry* **2011**, *966*, 284–298.

(2) Bessac, F.; Hoyau, S. Pesticide interaction with environmentally important cations: A theoretical study of atrazine in interaction with two Ca2+ cations. *Computational and Theoretical Chemistry* **2013**, *1022*, 6–13.

(3) Belzunces, B.; Hoyau, S.; Cuny, J.; Bessac, F. Pesticide interaction with environmentally important cations: A molecular dynamics and DFT study of metamitron and fenhexamid. *Computational and Theoretical Chemistry* **2017**, *1117*, 220–234.

(4) Belzunces, B.; Hoyau, S.; Benoit, M.; Tarrat, N.; Bessac, F. Theoretical study of the atrazine pesticide interaction with pyrophyllite and Ca2+ -montmorillonite clay surfaces. *Journal of Computational Chemistry* **2016**, *38*, 133–143.

(5) Belzunces, B.; Hoyau, S.; Bessac, F. Interaction of Metamitron and Fenhexamid with Ca2+-Montmorillonite Clay Surfaces: A Density Functional Theory Molecular Dynamics Study. *Journal of Computational Chemistry* **2019**, *40*, 1449–1462.

(6) Al-Mukhtar, M.; Qi, Y.; Alcover, J.-F.; Conard, J.; Bergaya, F. Hydromechanical effects: (II) on the water-Na-smectite system. *Clay Minerals* **2000**, *35*, 537–544.

(7) Hendricks, S. B.; Nelson, R. A.; Alexander, L. T. Hydration Mechanism of the Clay Mineral Montmorillonite Saturated with Various Cations1. *Journal of the American Chemical Society* **1940**, *62*, 1457–1464.

(8) El-Akkad, T.; Flex, N.; Guindy, N.; El-Massry, S.; Nashed, S. Nitrogen and water vapour adsorption on monovalent and divalent montmorillonite derivatives and their heats of immersion in polar liquid. *Surface Technology* **1982**, *17*, 69–77.

(9) Bishop, J.; Pieters, C.; Edwards, J. Infrared Spectroscopic Analyses on the Nature of Water in Montmorillonite. *Clays Clay Miner.* **1994**, *42*, 702–716.

(10) Xu, W.; Johnston, C.; Parker, P.; Agnew, S. Infrared Study of Water Sorption on Na-, Li-, Ca-, and Mg-Exchanged (SWy-1 and SAz-1) Montmorillonite. *Clays Clay Miner.* **2000**, *48*, 120–131.

(11) Sposito, G.; Prost, R.; Gaultier, J. Infrared Spectroscopic Study of Adsorbed Water on Reduced-Charge Na/Li-Montmorillonites. *Clays Clay Miner.* **1983**, *31*, 9–16.

(12) Zhang, G.; Al-Saidi, W. A.; Myshakin, E. M.; Jordan, K. D. Dispersion-Corrected Density Functional Theory and Classical Force Field Calculations of Water Loading on a Pyrophyllite(001) Surface. *The Journal of Physical Chemistry C* **2012**, *116*, 17134–17141.

(13) Mignon, P.; Ugliengo, P.; Sodupe, M.; Hernandez, E. R. Ab initio molecular dynamics study of the hydration of Li^+, Na^+ and K^+ in a montmorillonite model. Influence of isomorphic substitution. *Phys. Chem. Chem. Phys.* **2010**, *12*, 688–697.

(14) Berghout, A.; Tunega, D.; Zaoui, A. Density Functional Theory (DFT) Study of the Hydration Steps of Na+/Mg2+/Ca2+/Sr2+/Ba2+-Exchanged Montmorillonites. *Clays and Clay Minerals* **2010**, *58*, 174–187.

(15) Greathouse, J. A.; Storm, E. W. Calcium hydration on montmorillonite clay surfaces studied by Monte Carlo simulation. *Molecular Simulation* **2002**, *28*, 633–647.

(16) Sun, L.; Tanskanen, J. T.; Hirvi, J. T.; Kasa, S.; Schatz, T.; Pakkanen, T. A. Molecular dynamics study of montmorillonite crystalline swelling: Roles of interlayer cation species and water content. *Chemical Physics* **2015**, *455*, 23–31.

(17) Holmboe, M.; Bourg, I. C. Molecular Dynamics Simulations of Water and Sodium

Diffusion in Smectite Interlayer Nanopores as a Function of Pore Size and Temperature. *The Journal of Physical Chemistry C* **2014**, *118*, 1001–1013.

(18) Yang, G.; Neretnieks, I.; Holmboe, M. Atomistic simulations of cation hydration in sodium and calcium montmorillonite nanopores. *The Journal of Chemical Physics* **2017**, *147*, 084705.

(19) Badyal, Y. S.; Barnes, A. C.; Cuello, G. J.; Simonson, J. M. Understanding the Effects of Concentration on the Solvation Structure of Ca2+ in Aqueous Solution. II: Insights into Longer Range Order from Neutron Diffraction Isotope Substitution. *The Journal of Physical Chemistry A* **2004**, *108*, 11819–11827.

(20) Katz, A. K.; Glusker, J. P.; Beebe, S. A.; Bock, C. W. Calcium ion coordination: A comparison with that of Beryllium, Magnesium and Zinc. *Journal of the American Chemical Society* **1996**, *118*, 5752–5763.

(21) Ikeda, T.; Boero, M.; Terakura, K. Hydration properties of magnesium and calcium ions from constrained first principles molecular dynamics. *The Journal of Chemical Physics* **2007**, *127*, 074503.

(22) Adeagbo, W. A.; Doltsinis, N. L.; Burchard, M.; Maresch, W. V.; Fockenberg, T. Ca2+ solvation as a function of p, T, and pH from ab initio simulation. *The Journal of Chemical Physics* **2012**, *137*, 124502.

(23) Zhu, R.; Chen, Q.; Zhou, Q.; Xi, Y.; Zhu, J.; He, H. Adsorbents based on montmorillonite for contaminant removal from water: A review. *Applied Clay Science* **2016**, *123*, 239–258.

(24) Mignon, P.; Ugliengo, P.; Sodupe, M. Theoretical Study of the Adsorption of RNA/DNA Bases on the External Surfaces of Na+ -Montmorillonite. *J. Phys. Chem. C* **2009**, *113*, 13741–13749.

(25) Mignon, P.; Sodupe, M. Theoretical study of the adsorption of DNA bases on the acidic external surface of montmorillonite. *Phys. Chem. Chem. Phys.* **2012**, *14*, 945–954.

(26) Mignon, P.; Sodupe, M. Structural Behaviors of Cytosine into the Hydrated Interlayer of Na+ -Montmorillonite Clay. An ab Initio Molecular Dynamics Study. *J. Phys. Chem. C* **2013**, *117*, 26179–26189.

(27) Szczerba, M.; Kłapyta, Z.; Kalinichev, A. Ethylene glycol intercalation in smectites. Molecular dynamics simulation studies. *Applied Clay Science* **2014**, *91-92*, 87–97.

(28) Aggarwal, V.; Li, H.; Teppen, B. J. Triazine adsorption by saponite and beidellite clay minerals. *Environmental Toxicology and Chemistry* **2006**, *25*, 392.

(29) Clausen, P.; Andreoni, W.; Curioni, A.; Hughes, E.; Plummer, C. J. G. Adsorption of Low-Molecular-Weight Molecules on a Dry Clay Surface: An Ab Initio Study. *J. Phys. Chem. C* **2009**, *113*, 12293–12300.

(30) Tunega, D.; Gerzabek, M. H.; Haberhauer, G.; Lischka, H. Formation of 2,4–D complexes on montmorillonites – an ab initio molecular dynamics study. *European Journal of Soil Science* **2007**, *58*, 680–691.

(31) Myshakin, E. M.; Saidi, W. A.; Romanov, V. N.; Cygan, R. T.; Jordan, K. D. Molecular Dynamics Simulations of Carbon Dioxide Intercalation in Hydrated Na-Montmorillonite. *The Journal of Physical Chemistry C* **2013**, *117*, 11028–11039.

(32) Corbin, G.; Vulliet, E.; Lanson, B.; Rimola, A.; Mignon, P. Adsorption of Pharmaceuticals onto Smectite Clay Minerals: A Combined Experimental and Theoretical Study. *Minerals* **2021**, *11*, 62.

(33) Biswas, S.; Kwon, H.; Barsanti, K. C.; Myllys, N.; Smith, J. N.; Wong, B. M. Ab initio metadynamics calculations of dimethylamine for probing pKb variations in bulk vs. surface environments. *Phys. Chem. Chem. Phys.* **2020**, *22*, 26265–26277.

(34) Biswas, S.; Wong, B. M. High-Temperature Decomposition of Diisopropyl Methylphosphonate on Alumina: Mechanistic Predictions from Ab Initio Molecular Dynamics. *The Journal of Physical Chemistry C* **2021**, *125*, 21922–21932.

(35) Wardle, R.; Brindley, G. W. *American Mineralogist* **1972**, *57*, 732–750.

(36) Car, R.; Parrinello, M. Unified Approach for Molecular Dynamics and Density-Functional Theory. *Phys. Rev. Lett.* **1985**, *55*, 2471–2474.

(37) Kohn, W.; Sham, L. J. Self-Consistent Equations Including Exchange and Correlation Effects. *Phys. Rev.* **1965**, *140*, A1133–A1138.

(38) Perdew, J. P.; Burke, K.; Ernzerhof, M. Generalized Gradient Approximation Made Simple. *Phys. Rev. Lett.* **1996**, *77*, 3865–3868.

(39) Perdew, J. P.; Burke, K.; Ernzerhof, M. Erratum to Generalized Gradient Approximation Made Simple. *Phys. Rev. Lett.* **1997**, *78*, 1396–1396(E).

(40) Tunega, D.; Bučko, T.; Zaoui, A. Assessment of ten DFT methods in predicting structures of sheet silicates: Importance of dispersion corrections. *The Journal of Chemical Physics* **2012**, *137*, 114105.

(41) Voora, V. K.; Al-Saidi, W. A.; Jordan, K. D. Density Functional Theory Study of Pyrophyllite and M-Montmorillonites (M = Li, Na, K, Mg, and Ca): Role of Dispersion Interactions. *The Journal of Physical Chemistry A* **2011**, *115*, 9695–9703.

(42) CPMD, http://www.cpmd.org/, Copyright IBM Corp 1990-2015, Copyright MPI für Festkörperforschung Stuttgart 1997-2001.

(43) Grimme, S. Accurate description of van der Waals complexes by density functional theory including empirical corrections. *Journal of Computational Chemistry* **2004**, *25*, 1463–1473.

(44) Grimme, S. Semiempirical GGA-type density functional constructed with a long-range dispersion correction. *Journal of Computational Chemistry* **2006**, *27*, 1787–1799.

(45) Grimme, S.; Antony, J.; Ehrlich, S.; Krieg, H. A consistent and accurate ab initio parametrization of density functional dispersion correction (DFT-D) for the 94 elements H-Pu. *The Journal of Chemical Physics* **2010**, *132*, 154104.

(46) Hamann, D. R.; Schlüter, M.; Chiang, C. Norm-Conserving Pseudopotentials. *Physical Review Letters* **1979**, *43*, 1494–1497.

(47) Troullier, N.; Martins, J. L. Efficient pseudopotentials for plane-wave calculations. *Physical Review B* **1991**, *43*, 1993–2006.

(48) Monkhorst, H. J.; Pack, J. D. Special points for Brillouin-zone integrations. *Phys. Rev. B* **1976**, *13*, 5188–5192.

(49) Ceriotti, M.; Bussi, G.; Parrinello, M. Langevin Equation with Colored Noise for Constant-Temperature Molecular Dynamics Simulations. *Phys. Rev. Lett.* **2009**, *102*, 020601.

(50) Soper, A. The radial distribution functions of water and ice from 220 to 673 K and at pressures up to 400 MPa. *Chemical Physics* **2000**, *258*, 121–137.

(51) Skinner, L. B.; Huang, C.; Schlesinger, D.; Pettersson, L. G. M.; Nilsson, A.; Benmore, C. J. Benchmark oxygen-oxygen pair-distribution function of ambient water from x-ray diffraction measurements with a wide Q-range. *The Journal of Chemical Physics* **2013**, *138*, 074506.

(52) Bankura, A.; Karmakar, A.; Carnevale, V.; Chandra, A.; Klein, M. L. Structure, Dynamics, and Spectral Diffusion of Water from First-Principles Molecular Dynamics. *The Journal of Physical Chemistry C* **2014**, *118*, 29401–29411.

(53) Kirkwood, J. G. Statistical Mechanics of Fluid Mixtures. *The Journal of Chemical Physics* **1935**, *3*, 300–313.

(54) Torrie, G. M.; Valleau, J. P. Monte Carlo free energy estimates using non-Boltzmann sampling: Application to the sub-critical Lennard-Jones fluid. *Chemical Physics Letters* **1974**, *28*, 578–581.

(55) Torrie, G.; Valleau, J. Nonphysical sampling distributions in Monte Carlo free-energy estimation: Umbrella sampling. *Journal of Computational Physics* **1977**, *23*, 187–199.

(56) The PLUMED consortium, Promoting transparency and reproducibility in enhanced molecular simulations. *Nat. Methods* **2019**, *16*, 670.

(57) Tribello, G.; Bonomi, M.; Branduardi, D.; Camilloni, C.; Bussi, G. PLUMED2: New feathers for an old bird. *Comp. Phys. Comm.* **2014**, *185*, 604.

(58) Bonomi, M.; Branduardi, D.; Bussi, G.; Camilloni, C.; Provasi, D.; Raiteri, P.; Donadio, D.; Marinelli, F.; Pietrucci, F.; Broglia, R.; Parrinello, M. PLUMED: a portable plugin for free energy calculations with molecular dynamics. *Comp. Phys. Comm.* **2009**, *180*, 1961.

(59) Kollman, P. Free energy calculations: Applications to chemical and biochemical phenomena. *Chemical Reviews* **1993**, *93*, 2395–2417.

(60) Kumar, S.; Rosenberg, J. M.; Bouzida, D.; Swendsen, R. H.; Kollman, P. A. Multidimensional free-energy calculations using the weighted histogram analysis method. *Journal of Computational Chemistry* **1995**, *16*, 1339–1350.

(61) Roux, B. The calculation of the potential of mean force using computer simulations. *Computer Physics Communications* **1995**, *91*, 275–282.

(62) Trzesniak, D.; Kunz, A.-P. E.; van Gunsteren, W. F. A Comparison of Methods to Compute the Potential of Mean Force. *ChemPhysChem* **2007**, *8*, 162–169.

(63) Kumar, S.; Rosenberg, J. M.; Bouzida, D.; Swendsen, R. H.; Kollman, P. A. The weighted histogram analysis method for free-energy calculations on biomolecules. I. The method. *Journal of Computational Chemistry* **1992**, *13*, 1011–1021.

(64) Alan, G. "WHAM: the weighted histogram analysis method", version 2.0.9.1.

TOC Graphic

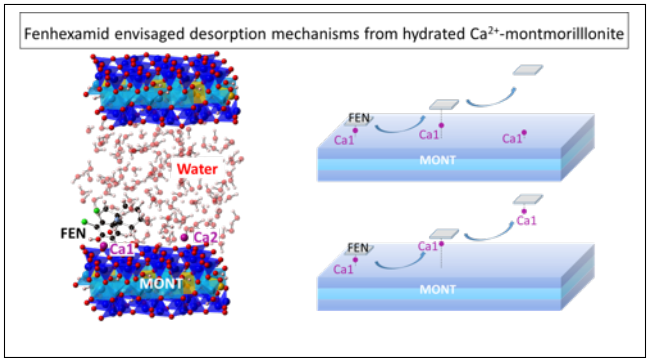
Fenhexamid envisaged desorption mechanisms from hydrated Ca2+-montmorilllonite
Water
FEN
Ca1
Ca2
MONT
FEN
Ca1
Ca1
Ca1
MONT
Ca1
FEN
Ca1
Ca1
MONT